

**Grand-canonical simulation of DNA condensation with two salts,  
affect of divalent counterion size**

Toan T. Nguyen<sup>1,2</sup>

<sup>1</sup>*Faculty of Physics,  
Hanoi University of Science,  
Vietnam National University,  
334 Nguyen Trai Street,  
Thanh Xuan, Hanoi, Vietnam*

<sup>2</sup>*School of Physics,  
Georgia Institute of Technology,  
837 State Street, Atlanta,  
Georgia 30332-0430, USA*

(Dated: September 16, 2018)

## Abstract

The problem of DNA–DNA interaction mediated by divalent counterions is studied using a generalized Grand-canonical Monte-Carlo simulation for a system of two salts. The effect of the divalent counterion size on the condensation behavior of the DNA bundle is investigated. Experimentally, it is known that multivalent counterions has strong effect on the DNA condensation phenomenon. While tri- and tetra-valent counterions are shown to easily condense free DNA molecules in solution into torroidal bundles, the situation with divalent counterions are not as clear cut. Some divalent counterions like  $\text{Mg}^{+2}$  are not able to condense free DNA molecules in solution, while some like  $\text{Mn}^{+2}$  can condense them into disorder bundles. In restricted environment such as in two dimensional system or inside viral capsid,  $\text{Mg}^{+2}$  can have strong effect and able to condense them, but the condensation varies qualitatively with different system, different coions. It has been suggested that divalent counterions can induce attraction between DNA molecules but the strength of the attraction is not strong enough to condense free DNA in solution. However, if the configuration entropy of DNA is restricted, these attractions are enough to cause appreciable effects. The variations among different divalent salts might be due to the hydration effect of the divalent counterions. In this paper, we try to understand this variation using a very simple parameters, the size of the divalent counterions. We investigate how divalent counterions with different sizes can leads to varying qualitative behavior of DNA condensation in restricted environments.

PACS numbers: 87.14.gk,87.19.xb,87.16.A-

## I. INTRODUCTION

The problem of DNA condensation in the presence of multivalent counterions has seen a strong revival of interest in recent years. This is because of the need to develop effective ways of gene delivery for the rapidly growing field of genetic therapy. DNA viruses such as bacteriophages provide excellent study candidates for this purpose. One can package genomic DNA into viruses, then deliver and release the molecule into targeted individual cells. Recently there is a large biophysical literature dedicated to the problem of DNA condensation (packaging and ejection) inside bacteriophages (for a review, see Ref. 1).

Because DNA is a strongly charged molecule in aqueous solution, electrostatics and the screening condition of the solution play an important role in the structure and functions of DNA systems. Specifically, the condensation of DNA molecules are strongly influenced by the counterion valence [2–5]. While tri- and tetra-valent counterions are shown to easily condense free DNA molecules in solution into toroidal bundles, the situation with divalent counterions are not as clear cut. Some divalent counterions like  $\text{Mg}^{+2}$  are not able to condense free DNA molecules in solution, while some like  $\text{Mn}^{+2}$  can condense them into disorder bundles. Similarly, strong electrostatic effect is also observed for DNA condensation in a restricted environment such as inside a viruses. By varying the salinity of solution, one can vary the amount of DNA ejected from viruses. Interestingly, monovalent counterions such as  $\text{Na}^{+1}$  have negligible effect on the DNA ejection process [6]. In contrast, multivalent counterions ( $Z$ -ions for short) such as  $\text{Mg}^{+2}$ ,  $\text{CoHex}^{+3}$ ,  $\text{Spd}^{+3}$  or  $\text{Spm}^{+4}$  exert strong and non-monotonic effects [7]. There is an optimal counterion concentration,  $c_{Z,0}$ , where the least DNA genome is ejected from the phages. For counterion concentration,  $c_Z$ , higher or lower than this optimal concentration, more DNA is ejected from phages. The case of divalent counterions is more marginal. The non-monotonicity is observed for  $\text{MgSO}_4$  salt but not for  $\text{MgCl}_2$  salt up to the concentration of 100mM. Such ion specificity for the case of divalent salts also present in condensation of DNA in free solution. [2].

The non-monotonic influence of multivalent counterions on DNA ejection from viruses is expected to have the same physical origin as the phenomenon of reentrant DNA condensation in free solution in the presence of counterions of tri-, tetra- and higher valence [8–12]. Although, divalent counterions are known to condense DNA only partially in free solution [2, 3], DNA virus provides an unique experimental setup. The constrain of the

viral capsid strongly eliminates configurational entropic cost of packaging DNA. This allows divalent counterions to influence DNA condensation similar to that of trivalent/tetravalent counterions. Indeed, DNA condensation by divalent counterions has also been observed in another environment where DNA configuration is constrained, namely the condensation of DNA in two dimensional systems [13]. For virus systems, theoretical fitting suggests that the DNA is neutralized at  $c_{Z,0} \approx 75\text{mM}$  for divalent counterions, and the short-range DNA attraction at this concentration is  $-0.004k_B T$  per nucleotide base [14, 15].

In this paper, we study the problem of DNA condensation in the presence of divalent counterions using computer simulations. The simulation method developed by our groups in Ref. 15, 16 are used, expanded and the influence of the ion size on the strength of DNA–DNA interaction mediated by divalent counterions are investigated [17]. The Grand Canonical Monte Carlo simulation for a system of two salts is presented in detail. The electrostatic contribution to the free energy of packaging DNA into bundles is calculated from simulation. It is shown that, if only the non-specific electrostatic contribution is included, divalent counterions can indeed induce DNA reentrant condensation like those observed for higher counterion valences. However, correlations among divalent counterions are not strong enough to de-condense DNA bundles. As already mentioned, experimental results also show that there is a ion specific effect. As a first step taken to study this ion specific effect, the DNA–DNA effective interaction is calculated from simulation for three different counterion sizes. It is shown that varying counterion sizes can have significant impact on DNA condensation pictures, which can explained some variations among DNA condensation experiments with  $\text{Mg}^{2+}$ , or  $\text{Mn}^{2+}$  counterions.

The paper is organized as follows. In Sec. II, the Grand-canonical Monte-Carlo is formulated to simulate a system of two salts (a divalent salts and a fixed monovalent salt from buffer solution). In Sec. III, the model of our system and various physical parameters used in the simulation are presented in details. In Sec. IV, the results are presented and their relevance to available experimental data are discussed. We conclude in Sec. V.

## II. GRAND CANONICAL MONTE–CARLO SIMULATION FOR MIXTURE OF TWO SALTS

In practical situation, the DNA bundle is in equilibrium with a water solution containing free mobile ions at given concentrations. Therefore we simulate the system using Grand Canonical Monte-Carlo (GCMC) simulation. The number of ions are not constant during the simulation. Instead their chemical potentials are fixed. These chemical potentials are chosen in advance by simulating a DNA–free salt solution and adjusting them so that the solution has the correct ion concentrations. Another factor that complicate the simulation of DNA condensation phenomenon arises from the fact that there are both monovalent and divalent salts in solution in experiments. At very low concentration of divalent counterions,  $c_Z$ , DNA is screened mostly by monovalent counterions. To properly simulate the DNA bundle at this low  $c_Z$  limit, and to properly capture the screening of electrostatic interactions among divalent counterions by monovalent ones, both salts are included in the simulations .

To simulate two different salts present in our system, the standard GCMC method for ionic solution [18] is generalized to simulate of a system containing a mixture of both multivalent and monovalent salts. For simplicity, we assume both salts have the same coion (for example,  $\text{Cl}^-$ ). Thus, a state  $i$  of the system is characterized by the locations of  $N_{iZ}$  multivalent counterions,  $N_{i+}$  monovalent counterions and  $N_{i-}$  coions. In the grand canonical ensemble of unlabeled particles, the probability of a such state is given by

$$\pi_i = \frac{1}{\mathcal{Z}} \frac{1}{\Lambda_Z^{3N_{iZ}} \Lambda_+^{3N_{i+}} \Lambda_-^{3N_{i-}}} \exp [\beta(\mu_Z N_{iZ} + \mu_+ N_{i+} + \mu_- N_{i-}) - \beta U_i] \quad (1)$$

Here,  $\mathcal{Z}$  is the grand canonical partition function,  $\beta = 1/k_B T$ ,  $\Lambda_{Z,+,-} \equiv h/\sqrt{2\pi m_{Z,+,-} k_B T}$ ,  $U_i$  is the interaction energy of the state  $i$ , and  $\mu_{Z,+,-}$  are the chemical potentials of the multivalent counterions, of the monovalent counterions and of the coions respectively.

In a Monte Carlo simulation, a Markov chain of system states  $i$  is generated with a limiting probability distribution proportional to  $\pi_i$ . This chain is defined by a probability  $p_{ij}$  of transitions from state  $i$  to state  $j$ . A sufficient condition for the Markov chain to have the correct limiting distribution is:

$$\frac{p_{ij}}{p_{ji}} = \frac{\pi_j}{\pi_i} \quad (2)$$

As usual, at each step of the chain, a “trial” move to change the system from state  $i$  to state

$j$  is attempted with probability  $q_{ij}$  and is accepted with probability  $f_{ij}$ . Clearly,

$$p_{ij} = q_{ij}f_{ij} \quad (3)$$

It is convenient to regard the simulation box as consisting of  $V$  discrete sites ( $V$  is very large). Then for a trial move where  $\nu_\alpha$  particles of species  $\alpha$  are added to the system:

$$q_{ij} = \frac{1}{V^{\nu_\alpha} \nu_\alpha!} \quad (4)$$

Conversely, if  $\nu_\alpha$  particles of species  $\alpha$  are removed from the system:

$$q_{ij} = \frac{(N_\alpha - \nu_\alpha)!}{N_\alpha! \nu_\alpha!} \quad (5)$$

Putting everything together, equations (1)–(5) give us a recipe to calculate the Metropolis acceptance probability of a particle insertion/deletion move in GCMC simulation. For example, if in a transition from state  $i$  to state  $j$ , a multivalent salt molecule (one  $Z$ -ion and  $Z$  coions) is added to the system, the Metropolis probability of acceptance of such move can be chosen as:

$$f_M = \min\{1, f_{ij}/f_{ji}\} \quad (6)$$

where

$$\frac{f_{ij}}{f_{ji}} = \frac{B_Z}{(N_{iZ} + 1)(N_{i-} + 1)\dots(N_{i-} + Z)} \exp[\beta(U_i - U_j)], \quad (7)$$

with

$$B_Z = \exp(\beta\mu_{Z,\text{salt}}) \frac{V^{Z+1}}{\Lambda_Z^3 \Lambda_-^{3Z}}, \quad (8)$$

and

$$\mu_{Z,\text{salt}} = \mu_Z + Z\mu_- \quad (9)$$

is the combined chemical potential of a multivalent salt molecule.

On the other hand, if a multivalent salt molecule (one  $Z$ -ion and  $Z$  coions) is removed from the system,

$$\frac{f_{ij}}{f_{ji}} = \frac{N_{iZ}N_{i-}\dots(N_{i-} - Z + 1)}{B_Z} \exp[\beta(U_i - U_j)], \quad (10)$$

Similarly, for addition a monovalent salt molecule (one monovalent counterion and one coion) in transition from state  $i$  to state  $j$ ,

$$\frac{f_{ij}}{f_{ji}} = \frac{B_1}{(N_{iZ} + 1)(N_{i-} + 1)} \exp[\beta(U_i - U_j)], \quad (11)$$

with

$$B_1 = \exp(\beta\mu_{1,\text{salt}}) \frac{V^2}{\Lambda_+^3 \Lambda_-^3}, \quad (12)$$

and

$$\mu_{1,\text{salt}} = \mu_+ + \mu_- \quad (13)$$

is the combined chemical potential of a monovalent salt molecule. For a “trial” move where a monovalent salt molecule is removed from the system,

$$\frac{f_{ij}}{f_{ji}} = \frac{N_{i+} N_{i-}}{B_1} \exp[\beta(U_i - U_j)], \quad (14)$$

Because we are trying to simulate a mixture of salts, to improve the system relaxation and to improve the sampling of the system’s phase space, one can also make a “trial” move where one  $Z$ -ion is added to the system and  $Z$  monovalent counterions are removed the system. For such move, it is easy to show that

$$\frac{f_{ij}}{f_{ji}} = \frac{B_1^Z N_{i+} \dots (N_{i+} - Z + 1)}{B_Z (N_{iZ} + 1)} \exp[\beta(U_i - U_j)], \quad (15)$$

Vice versas, for a “trial” move where one  $Z$ -ion is removed from the system and  $Z$  monovalent counterions are added to the system,

$$\frac{f_{ij}}{f_{ji}} = \frac{B_Z N_{iZ}}{B_1^Z (N_{i+} + 1) \dots (N_{i+} + Z)} \exp[\beta(U_i - U_j)]. \quad (16)$$

Note that because the system maintains charge neutrality in all particle addition/deletion moves, instead of using 3 different chemical potentials,  $\mu_{Z,+,-}$ , to simulate the system, only two combined chemical potentials,  $\mu_{Z,\text{salt}}$  and  $\mu_{1,\text{salt}}$ , are actually needed. In our actual implementation, the dimensionless parameters  $B_Z$  and  $B_1$ , Eqs. (12) and (8), are used instead of the chemical potentials themselves to simulate the DNA system. The values of these parameters for different mixtures of divalent and monovalent salts are listed in Sec. III, Table I.

Lastly, beside particle addition/deletion moves, one also try standard particle translation moves. They are carried out exactly like in the case of a canonical Monte-Carlo simulation. In a “trial” move from state  $i$  to state  $j$ , an ion is chosen at random and is moved to a random position in a volume element surrounding its original position. The standard Metropolis probability is used for the acceptance of such “trial” move:

$$f_M = \min\{1, \exp[\beta(U_i - U_j)]\}. \quad (17)$$

### III. THE SIMULATION MODEL

We model the DNA bundle in hexagonal packing as a number of DNA molecules arranged in parallel along the  $Z$ -axis. In the horizontal plane, the DNA molecules form a two dimensional hexagonal lattice with lattice constant  $d$  (the DNA–DNA interaxial distance) (Fig. 1). Individual DNA molecule is modeled as an impenetrable cylinder with negative charges

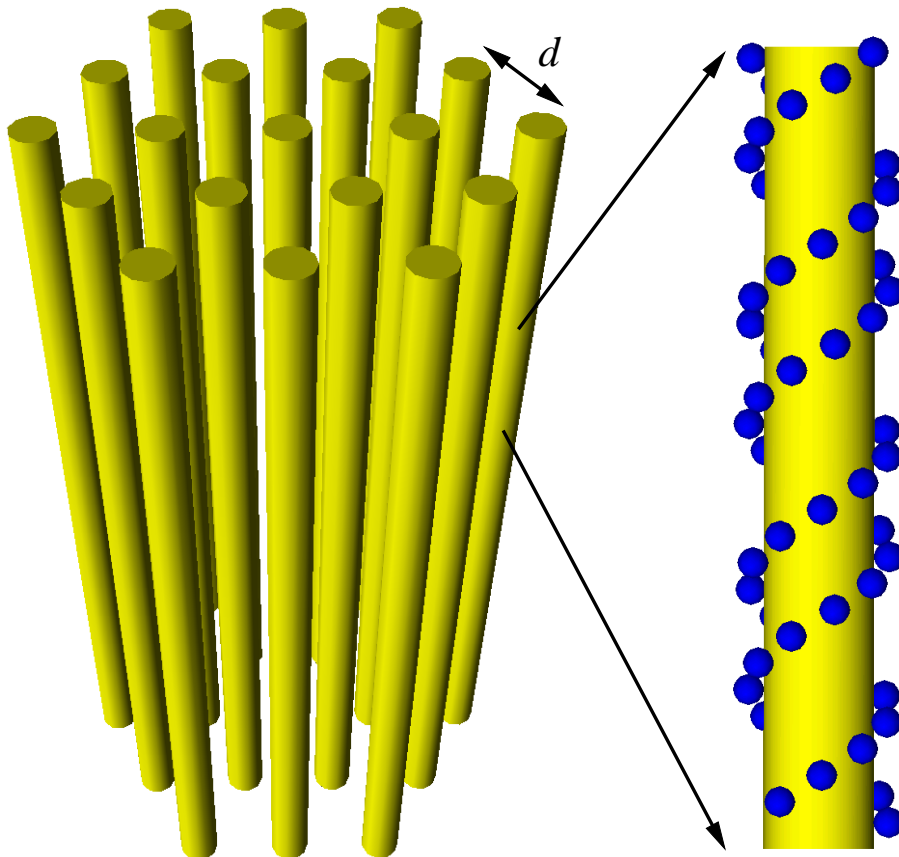


FIG. 1: (Color online) A DNA bundle is modeled as a hexagonal lattice with lattice constant  $d$ . Individual DNA molecule is modeled as a hard-core cylinder with negative charges glued on it according to the positions of nucleotides of a B–DNA structure.

glued on it. The charges are positioned in accordance with the locations of nucleotide groups along the double-helix structure of a B–DNA. The hardcore cylinder has radius of  $7\text{\AA}$ . The negative charges are hard spheres of radius  $2\text{\AA}$ , charge  $-e$  and lie at a distance of  $9\text{\AA}$  from the DNA axis. This gives an averaged DNA radius,  $r_{DNA}$ , of  $1\text{nm}$ . The solvent water is treated as a dielectric medium with dielectric constant  $\varepsilon = 78$  and temperature  $T = 300^\circ K$ . The positions of DNA molecules are fixed in space. This mimics the constrain on DNA



configurational entropy inside viruses and other experiments of DNA condensation using divalent counterions in restricted environment. The mobile ions in solution are modeled as hard spheres with unscreened Coulomb interaction (the primitive ion model). The coions have radius of  $\sigma_- = 2\text{\AA}$  and charge  $-e$ . The divalent counterions have radius of  $\sigma_Z = 2.0, 2.5, \text{ or } 3.0\text{\AA}$  and charge  $+2e$ . The interaction between two ions  $\alpha$  and  $\beta$  with radii  $\sigma_{\alpha,\beta}$  and charges  $Q_{\alpha,\beta}$  is given by

$$U = \begin{cases} Q_\alpha Q_\beta / \epsilon r_{\alpha\beta} & \text{if } r_{\alpha\beta} > \sigma_\alpha + \sigma_\beta \\ \infty & \text{if } r_{\alpha\beta} < \sigma_\alpha + \sigma_\beta \end{cases} \quad (18)$$

where  $r_{\alpha\beta} = |\mathbf{r}_\alpha - \mathbf{r}_\beta|$  is the distance between the ions.

The simulation is carried out using the periodic boundary condition. Unless explicitly stated, a periodic simulation cell with  $N_{DNA} = 12$  DNA molecules in the horizontal ( $x, y$ ) plane and 3 full helix periods in the  $z$  direction is used. The dimensions of the box are  $L_x = 3d$ ,  $L_y = 2\sqrt{3}d$  and  $L_z = 102\text{\AA}$ . This gives, for the volume of the simulation box,

$$V_{\text{cell}} = 612\sqrt{3} d^2 \text{\AA}^3 \quad (19)$$

The long-range electrostatic interactions between charges in neighboring cells are treated using the Ewald summation method. In Ref. [19, 20], it is shown that the macroscopic limit is reached when  $N_{DNA} \geq 7$ . Our simulation cell contains 12 DNA helices, hence it has enough DNA molecules to eliminate the finite size effect. Test runs with 1, 4, 7 and 12 DNA molecules are carried out to verify that this is indeed the case.

As mentioned above, the DNA bundle is simulated in equilibrium with a bulk solution containing two salt concentrations: a varying bulk multivalent counterion concentrations  $c_Z$  and a fixed bulk concentration of monovalent salt,  $c_1 = 50\text{mM}$ . The detail implementation of the GCMC method for this case is described in section II. The number of ions are not constant during the simulation. Instead their chemical potentials are fixed. These chemical potentials are chosen in advance by simulating a DNA-free salt solution and adjusting them so that the solution has the correct ion concentrations. In simulation, the chemical potential of each salt is set by fixing the parameters  $B_{1,Z}$  given by Eq. (8, 12).

In Table I, various values for the parameters  $B_Z^*$  and  $B_1^*$  that are used in this work for divalent counterion size of  $2\text{\AA}$  are shown. These values are listed for a reference volume  $V_{\text{cell}}^*$  that is chosen to have the same dimensions as that of a DNA bundle system with

$B_Z^*$	$B_1^*$	$c_Z$ (mM)	$c_1$ (mM)	$P_b$ (atm)
$0.744 \times 10^5$	$0.612 \times 10^4$	$13.9 \pm 3.0$	$50.0 \pm 5.6$	$3.183 \pm 0.001$
$2.568 \times 10^5$	$0.808 \times 10^4$	$29.9 \pm 3.4$	$50.2 \pm 4.9$	$4.17 \pm 0.01$
$14.48 \times 10^5$	$1.306 \times 10^4$	$74.6 \pm 6.2$	$50.1 \pm 5.3$	$6.874 \pm 0.006$
$26.43 \times 10^5$	$1.580 \times 10^4$	$99.8 \pm 5.7$	$50.3 \pm 5.4$	$8.391 \pm 0.006$
$56.67 \times 10^5$	$2.128 \times 10^4$	$150.2 \pm 8.4$	$50.6 \pm 6.7$	$11.42 \pm 0.02$
$323.82 \times 10^5$	$3.715 \times 10^4$	$299.6 \pm 11.2$	$49.4 \pm 6.8$	$20.81 \pm 0.04$
$1302.73 \times 10^5$	$6.601 \times 10^4$	$507.1 \pm 13.6$	$50.3 \pm 6.9$	$35.0 \pm 0.1$

TABLE I: The parameters,  $B_Z^*$  and  $B_1^*$ , of the salts used in the simulation for the reference volume  $V_{\text{cell}}^* \simeq 2.65 \times 10^6 \text{ \AA}^3$  (see text for detail). Columns 3 and 4 show the corresponding salt concentrations of the simulated DNA-free bulk solution. Column 5 shows the total pressure of the bulk solutions obtained from simulation.

$d = 50 \text{ \AA}$ , so  $V_{\text{cell}}^* \simeq 2.65 \times 10^6 \text{ \AA}^3$ . For a simulation system where  $d$  is different from  $50 \text{ \AA}$ , the parameters  $B_Z$  and  $B_1$  are scaled correspondingly:

$$B_Z(d) = B_Z^* \left( \frac{d}{50 \text{ \AA}} \right)^{2Z+2}, B_1(d) = B_1^* \left( \frac{d}{50 \text{ \AA}} \right)^4. \quad (20)$$

In columns 3 and 4 of table I, the resultant salt concentrations,  $c_Z$  and  $c_1$ , of the DNA-free solution obtained from our GCMC simulations are listed. The divalent salt concentration is varied from 14 mM to 507 mM while the monovalent salt concentration is kept at approximately 50 mM. Typical standard deviations in the concentration is about 10% in our simulation. This relative error is in line with previous GCMC simulations of primitive electrolytes [18]. Note that, even though  $c_1$  is kept constant,  $B_1^*$ , (and correspondingly the monovalent salt chemical potential  $\mu_{1,\text{salt}}$ ) is not a constant but actually increases with  $c_Z$ . This is expected because higher  $c_Z$  leads to higher free energy cost of adding a monovalent salt to the system.

For each simulation run, about 500-1000 millions MC moves are carried out depending on the averaged number of ions in the system. To ensure thermalization, about 50 millions initial moves are discarded before doing statistical analysis of the result of the simulation.

In this paper, we are concerned with calculating the “effective” DNA–DNA interaction, and correspondingly the free energy of assembling DNA bundle. In general, this is not a

trivial task for a Monte-Carlo simulation because the entropy cannot be calculated explicitly. To overcome this problem, the Expanded Ensemble method [19] is implemented. This method allows us to calculate the difference of the system free energies at different volumes by sampling these volumes simultaneously in a simulation run. By sampling two nearly equal volumes,  $V$  and  $V + \Delta V$ , and calculate the free energy difference  $\Delta\Omega$ , we can calculate the total pressure of the system:

$$P(T, V, \{\mu_\nu\}) = - \left. \frac{\partial\Omega(T, V, \{\mu_\nu\})}{\partial V} \right|_{T, \{\mu_\nu\}} \simeq - \frac{\Delta\Omega}{\Delta V} \quad (21)$$

Here  $\{\mu_\nu\} = \{\mu_Z, \mu_1, \mu_{-1}\}$  are the set of chemical potentials of different ion species. The osmotic pressure of the DNA bundle is then obtained by subtracting the total pressure of the bulk DNA-free solution,  $P_b(T, V, \{\mu_\nu\})$ , from the total pressure of the DNA system:

$$P_{osm}(T, V, \{\mu_\nu\}) = P(T, V, \{\mu_\nu\}) - P_b(T, V, \{\mu_\nu\}) \quad (22)$$

The total pressure of the bulk solution,  $P_b(T, V, \{\mu_\nu\})$ , needs to be calculated only once for each set of salt concentrations,  $c_Z$  and  $c_1$ . For reference purpose, their values are listed in column 5 of Table I.

All simulations are done using the physics simulation library SimEngine develop by one of the author (TTN). This library use OpenCL and OpenMP extensions of the C programming language to distribute computational workloads on multi-core CPU and GPGPU to speed up the simulation time. Both molecular dynamics and Monte-Carlo simulation methods are supported. In this paper the Monte-Carlo module of the library is used.

## IV. RESULT AND DISCUSSION

### A. Counterion mediated DNA–DNA interactions and the DNA packaging free energy

In Fig. 2, the osmotic pressure of DNA bundle at different  $c_Z$  is plotted as a function of the interaxial DNA distance,  $d$  for the case the counterion size is  $2\text{\AA}$ . Because this osmotic pressure is directly related to the “effective” force between DNA molecules at that interaxial distance [19, 20], this figure also serves as a plot of DNA–DNA interaction. As one can see, when  $c_Z$  is greater than a value around 20mM, there is a short–range attraction between two DNA molecules as they approach each other. This is the well-known

phenomenon of like-charge attraction between macroions [11, 12, 21]. It is the result of the electrostatic correlations between counterions condensed on the surface of each DNA molecule. The attraction appears when the distance between these surfaces is of the order of the lateral separation between counterions (about  $14\text{\AA}$  for divalent counterions). The maximal attraction occurs at the distance  $d \simeq 27\text{\AA}$ , in good agreement with various theoretical and experimental results [2, 22]. For smaller  $d$ , the DNA-DNA interaction experiences sharp increase. This can be understood as the result of the hardcore repulsion between the counterions.

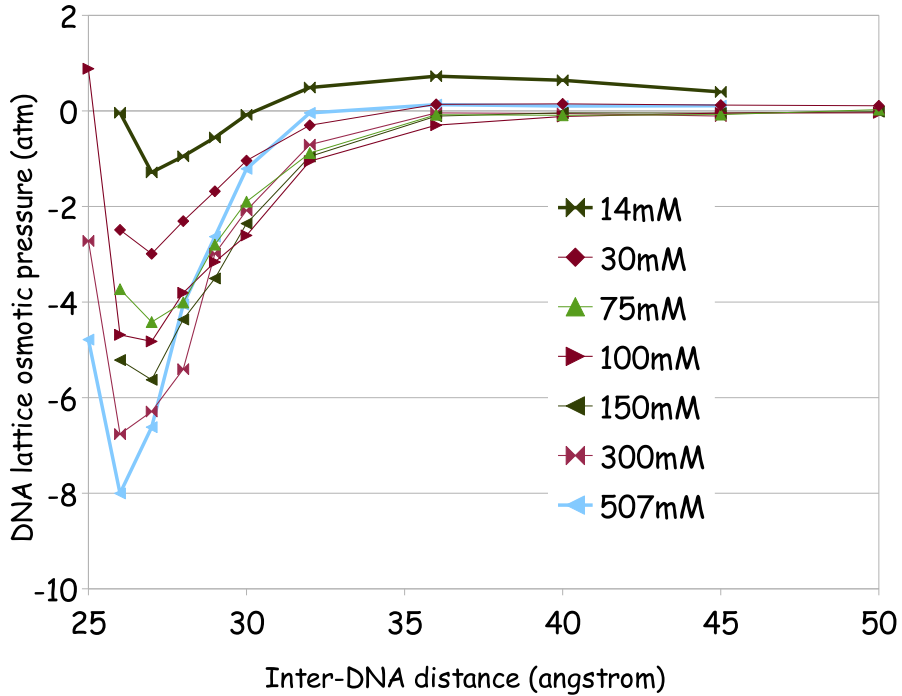


FIG. 2: (Color online) The osmotic pressure of the DNA bundle as function of the interaxial DNA distance  $d$  for different divalent counterion concentration  $c_z$  shown in the inset. The solid lines are guides to the eye. The counterion radius is  $2.0\text{\AA}$

From the P-V curve, we can also calculate the free energy,  $\mu_{\text{DNA}}$ , of packaging DNA into bundles. This free energy is nothing but the difference between the free energy of a DNA molecule in a bundle and that of an individual DNA molecule in the bulk solution ( $d = \infty$ ). It can be calculated by integrating the pressure with the volume of the bundle. Per DNA nucleotide base, the packaging free energy is given by:

$$\mu_{\text{DNA}}(d) = \frac{l}{L_z N_{\text{DNA}}} \int_{\infty}^d P_{\text{osm}}(d') dV = \frac{l}{N_{\text{DNA}}} \int_{\infty}^d P_{\text{osm}}(d') \frac{2L_x L_y}{d'} dd' \quad (23)$$

here  $l = 1.7\text{\AA}$  is the distance between DNA nucleotides along the axis of the DNA. The numerical result for  $\mu_{\text{DNA}}(d^*)$  at the optimal bundle lattice constant  $d^*$  is plotted in Fig. 3 as function of the  $c_Z$ . Due to the limitation of computer simulations, the numerical integration is performed up to the distance  $d = 50\text{\AA}$  only. However, this will not change the conclusion of this paper because the omitted integration from  $d = 50\text{\AA}$  to  $d = \infty$  only gives an almost constant shift to  $\mu_{\text{DNA}}$ . As evident from Fig. 3, the non-monotonic

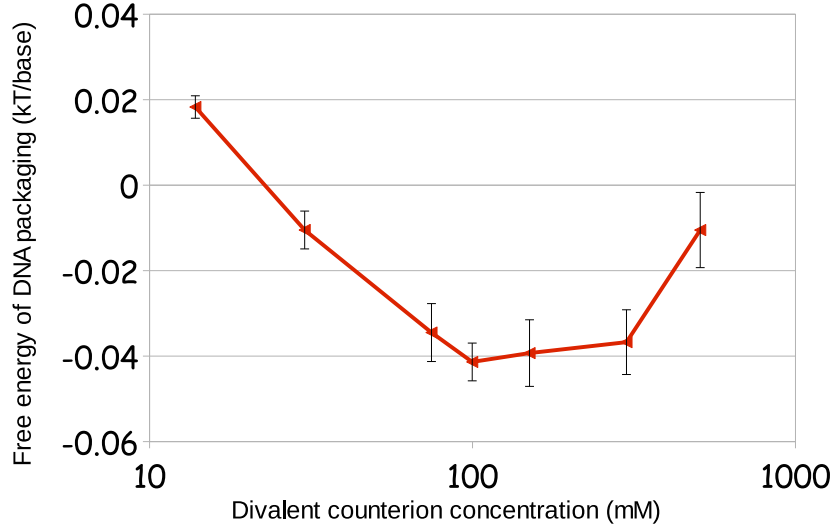


FIG. 3: (Color online) The free energy of packaging DNA molecules into hexagonal bundles as a function of the divalent counterion concentrations. The points are results of numerical integration of  $P_{osm}$  from Fig. 3.

dependence of the electrostatic contribution to DNA packaging free energy is clearly shown. There is an optimal concentration,  $c_{Z,0}$ , where the free energy cost of packaging DNA is lowest. It is even negative indicating the tendency of the divalent counterions to condense the DNA. At smaller or larger concentrations of the counterions, the free energy cost of DNA packaging is higher. These results are consistent with the correlation theory of DNA reentrant condensation by multivalent counterions [8, 21, 23] and the experiment results on ejecting DNA from bacteriophage under varying counterion concentrations [7]. However, it must be stated, unlike the condensation with counterions of higher valence [24], the divalent counterions in our simulation are not able to decondense the DNA bundle within the range of concentration considered. The free energy does not become positive beyond  $c_{Z,0}$ . This is in line with experimental results [2].

Figure 3 gives the short-range attraction among DNA molecules to be  $-0.04k_B T/\text{base}$ . This is larger than the fitted value obtained from the viral DNA ejection experiments [14]. There are many factors that leads to this quantitative discrepancy. Our main approximation is that in the simulation, the position of the DNA cylinders are straight with infinite bending rigidity. Inside viruses, DNA are bent, and the configuration entropy of the DNA are not necessary zero, and there is not a perfect hexagonal arrangement of DNA cylinder with fixed inter-DNA distance. We also neglect the contribution from the region  $d > 50\text{\AA}$  in our integration. The physical parameters of the system such as ion sizes, DNA orientations (twisting, frustrations),... [5, 25, 26] can also affect the strength of DNA-DNA short range attraction. All these factors are expected to reduce the attraction between the DNA compared to our idealized simulation. Nevertheless, the non-monotonic electrostatic influence of divalent counterions on DNA-DNA “effective” interaction is clearly demonstrated in our idealized simulation.

### B. Role of finite size of counterions

In all the systems simulated so far, the radius of the divalent counterion is fixed at  $2.0\text{\AA}$ . The results agree qualitatively and semi-quantitatively with some of the experimental results of DNA ejection from capsid with  $\text{MgSO}_4$  salt. However, experimental results also show that there is an ion specific effect. There are some significant differences in condensations of free DNA, condensations of DNA inside viruses when different divalent salts such as  $\text{MgSO}_4$ ,  $\text{MgCl}_2$ , or  $\text{MnCl}_2$  are used[2, 6]. This shows that the hydration effect, and the entropy of the hydrated water molecules are significant and need to be properly taken into account when one deals with the problem of DNA confinement inside viral capsids. In this section, a first step is taken to study this ion specific effect. Specifically, we study how DNA-DNA interaction is affected by changing the radius of the counterions.

In Fig. 4, and Fig. 5, the dependence of DNA-DNA “effective” interaction on the DNA-DNA separation distance are plotted for the counterion radii  $2.5\text{\AA}$  and  $3\text{\AA}$  respectively. Compare to similar plot for the case of  $\sigma_Z = 2.0\text{\AA}$  (Fig. 2), we can clearly see that the main physics remains when we change the counterion size. The DNA-DNA short-range interaction remains evident. However, the depth and location of the strongest attraction changes when the counterion size changes. The smallest counterions ( $2\text{\AA}$ ) cause the strongest attraction

among DNA at smaller distance. This is easily understood, the smaller counterion cause less entropic cost of bringing DNA closer to each other. Hence the short-range attraction is enhanced.

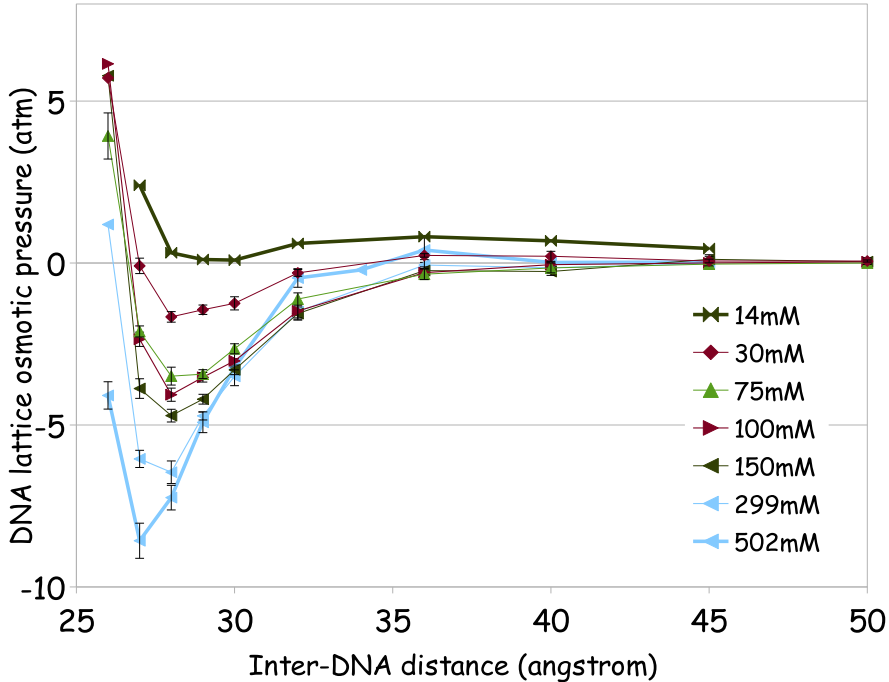


FIG. 4: (Color online) The osmotic pressure of the DNA bundle as function of the interaxial DNA distance  $d$  for different divalent counterion concentration  $c_Z$  shown in the inset. The solid lines are guides to the eye. The counterion radius is  $2.0 \text{ \AA}$

The change in the equilibrium separation of DNA in the bundle is even more evident in Fig. 6. In this figure, the osmotic pressure (which is proportional to the effective DNA–DNA interaction) of the hexagonal DNA bundle is plotted as a function of the inter DNA distance for three counterion sizes,  $2\text{\AA}$ ,  $2.5\text{\AA}$ , and  $3\text{\AA}$ , respectively. The counterion concentration is chosen to be approximately  $150\text{mM}$  in each simulation. As one can see, the first consequence of changing counterion size is obviously the equilibrium distance of the DNA bundle. The optimal inter DNA distance,  $d^*$ , where the short range DNA attraction is strongest increases with the counterion radius. As the counterion radius is increased from  $2.0\text{\AA}$  to  $2.5\text{\AA}$  to  $3.0\text{\AA}$   $d^*$  increases from  $26\text{\AA}$  to  $27\text{\AA}$  then  $29\text{\AA}$  respectively.

However, it is an interesting observation that not only the optimum distance  $d^*$  is shifted by  $2\sigma_Z$ , the interaction between DNA molecules from the distance  $d^*$  to  $\infty$ , which is dom-

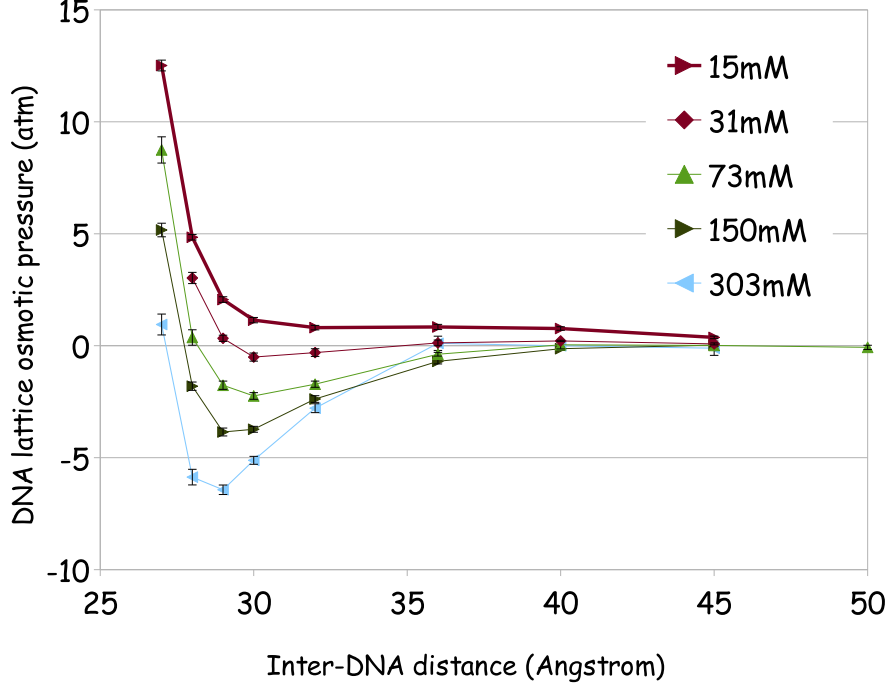


FIG. 5: (Color online) The osmotic pressure of the DNA bundle as function of the interaxial DNA distance  $d$  for different divalent counterion concentration  $c_Z$  shown in the inset. The solid lines are guides to the eye. The counterion radius is  $\sigma_Z = 3.0\text{\AA}$

inated by electrostatics, is shifted by the same amount. This is in agreement with the “correlated liquid” nature of DNA–DNA attraction mediated by multivalent counterions [15, 21]. In this strongly correlated liquid theory of DNA–DNA interaction, the combined system of DNA+condensed counterions acts as a charged metallic cylinder. The correlations between the condensed counterions on the surface of two neighboring DNA induce a short range attraction between them. In this theory, the center of mass of condensed counterion cannot approach the DNA surface at a distance less than its radius,  $\sigma_Z$ . Because of this, the *effective* surface of the dressed metallic DNA is lifted off the *bare* DNA surface by a distance of

$$x = \sigma_Z + \lambda + |\xi|, \quad (24)$$

where  $\lambda$  is the Goy-Chapman length. The length  $\xi$  is half the (negative) screening length of the strongly correlated liquid of the condensed counterions on the surface of the DNA molecule.

$$\xi = \frac{\varepsilon}{4\pi(Ze)^2} \frac{d\mu}{dn} \quad (25)$$



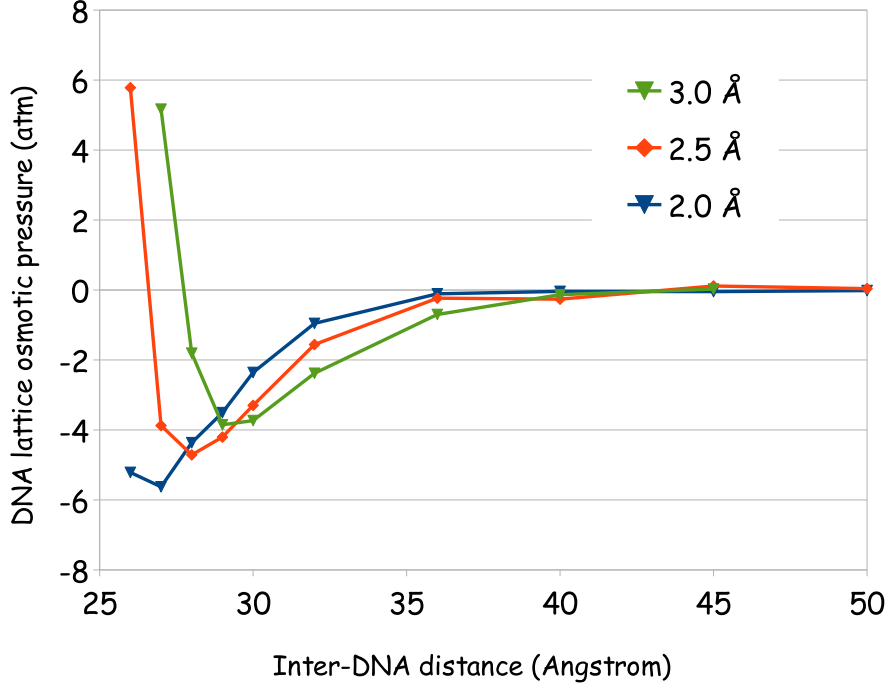


FIG. 6: (Color online) The osmotic pressure of the DNA hexagonal bundle as function of the lattice constant,  $d$ , for three values of the counterion radius. Equilibrium positions of DNA molecules increases roughly by  $2\sigma$  as the counterion radius increases. The attractive electrostatic interaction is also shifted as well.

with  $\mu$  the chemical potential of a counterion in the liquid, and  $n$  is its two-dimensional density. This screening length,  $|\xi|$ , depends weakly on the ratio,  $\sigma_Z/r_{DNA}$ . For our purpose, it can be considered to be constant. Thus, the electrostatic interaction between two neighboring DNA cylinders to be shifted by a distance of  $2\sigma_Z$  when the radius of the counterion changes. This agrees with our simulation results.

In Fig. 7, the free energy of packaging DNA into an hexagonal bundle with the optimal inter-DNA distance,  $d^*$ , is plotted as a function of the counterion concentrations for the three different counterion radii. It can be seen clearly that, within the range of counterion concentration studied, there is a quantitative and qualitative difference in the free energy of packaging for the three sizes of counterion consider. For  $\sigma_Z = 2\text{\AA}$  and  $2.5\text{\AA}$ , the dependence of the free energy of packaging DNA in bundle on the concentration  $c_Z$  is non-monotonic. However, for the larger counterion size,  $\sigma_Z = 3\text{\AA}$ , in the range of concentration considered, DNA condense later but stronger into hexagonal bundle as the counterion concentration

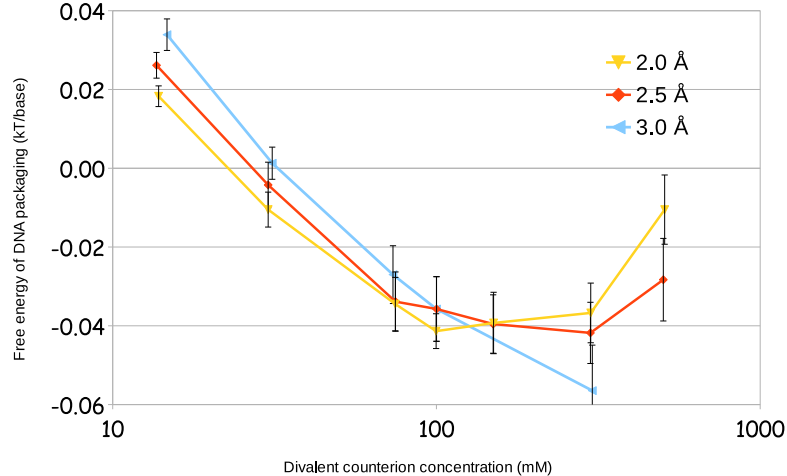


FIG. 7: Free energy per nucleotide base of packaging DNA molecules into bundles as a function of counterion concentration  $c_Z$  for different radii of the counterions.

increases. This behavior is actually observed in experiments. While the non-monotonic behaviors of DNA ejection is observed clearly for  $\text{MgSO}_4$  salt, and somewhat evident for  $\text{MgCl}_2$  salt,  $\text{MnCl}_2$  are known to condense DNA in free solution without ever disintegrated [2, 7]. Our simulation suggests that the difference in the hydration radius of the counterions can be used to explain such differences.

## V. CONCLUSION

In this paper, we use a Grand-Canonical Monte-Carlo simulation to study the electrostatics of DNA condensation, using a primitive model for the screen ions. Specifically, the effective electrostatic interaction between DNA molecules in a hexagonal bundle is computed in the presence of 50mM monovalent counterions and with varying concentration of divalent counterions. The entropy of DNA configure fluctuation is suppressed in simulation by fixing the position of the DNA cylinders in the bundle. Such study can be applied directly to the experimental problem of DNA ejection from bacteriophages where DNA condensed in a strongly confined environment. It is shown that, even at the level of non-specific electrostatic interaction, divalent counterions can strongly influence DNA interaction and packaging. The simulation results for divalent counterions with 2.0Å radius show that the electrostatic free energy of packaging DNA into hexagonal bundle varies non-monotonically with the counte-

monomer concentration. However, divalent counterions do not correlate strongly enough with each other to drive DNA de-condensation. The counterion specificity such as the ion hydration radius can influence strongly the qualitative and quantitative picture of DNA condensation. Three different counterion sizes are studied. They show that the non-monotonicity changes significantly and disappears as the counterion size increases. This is also in agreement with experiments. Going beyond the scope of DNA ejection experiments, we believe the quantitative results of our paper can be used to understand many other experiments involving DNA and divalent counterions.

### Acknowledgments

We would like to thank Lyubartsev, Shklovskii, Evilevich, Fang, Gelbart for valuable discussions. TTN acknowledges the financial support of the Vietnam National Foundation for Science and Technology NAFOSTED Contract 103.02-2012.75 and the USA National Science Foundation grant NSF CBET-1134398. The authors are indebted to A. Lyubartsev for providing us with the source code of their Expanded Ensemble Method.

- 
- [1] C. M. Knobler and W. M. Gelbart, *Annu. Rev. Phys. Chem.* **60**, 367 (2009).
  - [2] D. C. Rau and V. A. Parsegian, *Biophys. J.* **61**, 246 (1992).
  - [3] N. V. Hud and K. H. Downing, *Proc. Nat. Acad. Sci. USA* **98**, 14925 (2001).
  - [4] T. X. Hoang, A. Giacometti, R. Podgornik, N. T. T. Nguyen, J. R. Banavar, and A. Maritan, *J. Chem. Phys.* **140**, 064902 (2014).
  - [5] G. M. Grason, *Phys. Rev. Lett.* **105**, 045502 (2010).
  - [6] A. Evilevitch, L. Lavelle, C. M. Knobler, E. Raspaud, and W. M. Gelbart, *Proc. Nat. Acad. Sci. USA* **100**, 9292 (2003).
  - [7] A. Evilevitch, L. T. Fang, A. M. Yoffe, M. Castelnovo, D. C. Rau, V. A. Parsegian, W. M. Gelbart, and C. M. Knobler, *Biophys. J.* **94**, 1110 (2008).
  - [8] T. T. Nguyen, I. Rouzina, and B. I. Shklovskii, *J. Chem. Phys.* **112**, 2562 (2000).
  - [9] M. Saminathan, T. Antony, A. Shirahata, L. H. Sigal, T. Thomas, and T. J. Thomas, *Biochemistry* **38**, 38213830 (1999).

- [10] J. Pelta, D. Durand, J. Doucet, and F. Livolant, *Biophys. J.* **71**, 48 (1996).
- [11] A. Naji, A. Arnold, C. Holm, and R. R. Netz, *Eur. Phys. Lett.* **67**, 130 (2004).
- [12] W. M. Gelbart, R. F. Bruinsma, P. A. Pincus, and A. V. Parsegian, *Phys. Today* **53**, 38 (2000).
- [13] I. Koltover, K. Wagner, and C. R. Safinya, *Proc. Nat. Acad. Sci. USA* **97**, 14046 (2000).
- [14] S. Lee, C. V. Tran, and T. T. Nguyen, *J. Chem Phys.* **134**, 125104 (2011), cond-mat/0811.1296.
- [15] T. T. Nguyen, *J. Biol. Phys.* **39**, 247 (2013).
- [16] S. Lee, T. T. Le, and T. T. Nguyen, *Phys. Rev. Lett.* **105**, 248101 (2010).
- [17] Some of our results for the case of  $\sigma_Z = 2.5\text{\AA}$  has been presented in earlier work[16]. In this work, the normalization are changed. When exchange ions with bulk solution, salts are added to the whole volume instead of avoiding DNA volume . This does not change the conclusions of the papers, however, the attraction is stronger. The updated data is presented in this paper in section IVa.
- [18] J. P. Valleau and L. K. Cohen, *J. Chem. Phys.* **72**, 5935 (1980).
- [19] A. P. Lyubartsev and L. Nordenskiöld, *J. Phys. Chem.* **99**, 10373 (1995).
- [20] L. Guldbrand, L. G. Nilsson, and L. Nordenskiöld, *J. Chem. Phys.* **85**, 6686 (1986).
- [21] A. Y. Grosberg, T. T. Nguyen, and B. Shklovskii, *Rev. Mod. Phys.* **74**, 329 (2002).
- [22] P. K. Purohit, M. M. Inamdar, P. D. Grayson, T. M. Squires, J. Kondev, and R. Phillips, *Biophys. J.* **88**, 851 (2005).
- [23] B. I. Shklovskii, *Phys. Rev. E* **60**, 5802 (1999).
- [24] T. T. Nguyen, I. Rouzina, and B. I. Shklovskii, *J. Chem. Phys.* **112**, 2562 (2000).
- [25] N. Grønbech-Jensen, R. J. Mashl, R. F. Bruinsma, and W. M. Gelbart, *Phys. Rev. Lett.* **78**, 24772480 (1997).
- [26] A. P. Lyubartsev, J. X. Tang, P. A. Janmey, and L. Nordenskiöld, *Phys. Rev. Lett.* **81**, 5465 (1998).